



Arctic microbial community dynamics influenced by elevated CO₂ levels

C. P. D. Brussaard¹, A. A. M. Noordeloos¹, H. Witte¹, M. C. J. Collenteur¹, K. Schulz², A. Ludwig², and U. Riebesell²

¹Department of Biological Oceanography, NIOZ - Royal Netherlands Institute for Sea Research, PO Box 59, 1790 AB Den Burg, Texel, The Netherlands

²Helmholtz Centre for Ocean Research (GEOMAR), Kiel, Germany

Correspondence to: C. P. D. Brussaard (corina.brussaard@nioz.nl)

Received: 10 August 2012 – Published in Biogeosciences Discuss.: 12 September 2012

Revised: 21 December 2012 – Accepted: 2 January 2013 – Published: 1 February 2013

Abstract. The Arctic Ocean ecosystem is particularly vulnerable to ocean acidification (OA) related alterations due to the relatively high CO₂ solubility and low carbonate saturation states of its cold surface waters. Thus far, however, there is only little known about the consequences of OA on the base of the food web. In a mesocosm CO₂-enrichment experiment (overall CO₂ levels ranged from ~180 to 1100 μatm) in Kongsfjorden off Svalbard, we studied the consequences of OA on a natural pelagic microbial community. OA distinctly affected the composition and growth of the Arctic phytoplankton community, i.e. the picoeukaryotic photoautotrophs and to a lesser extent the nanophytoplankton thrived. A shift towards the smallest phytoplankton as a result of OA will have direct consequences for the structure and functioning of the pelagic food web and thus for the biogeochemical cycles. Besides being grazed, the dominant pico- and nanophytoplankton groups were found prone to viral lysis, thereby shunting the carbon accumulation in living organisms into the dissolved pools of organic carbon and subsequently affecting the efficiency of the biological pump in these Arctic waters.

surface water pH values were still 8.2 just prior to the industrial era, they are 8.11 at present and anticipated to reach 7.8 in the year 2100 (The Royal Society, 2005). This corresponds to CO₂ levels of 380 μatm at present to a projected high of at least 750 μatm by the end of this century.

Changes in carbonate chemistry can be expected to directly affect phytoplankton photosynthesis and subsequently growth because of their dependence on CO₂ supply. Not all algal groups will be equally affected, as certain groups (most notably diatoms) have developed CO₂-concentrating mechanisms (CCMs). However, algal species differ in CCM efficiency (Rost et al., 2008). Non-calcifying phytoplankton show, as expected, a range of responses, varying from no effect on growth to stimulating or adverse effect on growth or primary production (Riebesell and Tortell, 2011). Only a few studies have reported on OA-induced changes of phytoplankton community composition (Tortell et al., 2002; Engel et al., 2008; Meakin and Wyman, 2011; Feng et al., 2009), and the ecological consequences of OA on natural phytoplankton dynamics are still understudied.

Furthermore, a major gap in our understanding concerns the transfer of responses from the organism to the community and ecosystem levels. Rose et al. (2009) recently showed that climate change variables (temperature and *p*CO₂) did affect trophic dynamics during a North Atlantic spring bloom. As a result, predicting the impact of ocean acidification on marine ecosystem dynamics, and consequently biogeochemically cycling, is presently still limited. As pointed out by The Royal Society (2005), marine ecosystems are likely to become less robust as a result of ocean acidification and will be more vulnerable to other environmental changes

1 Introduction

The increase of *p*CO₂ in the surface ocean (ocean acidification, OA) profoundly affects the seawater carbonate system through well-known chemical reactions, lowering the pH, increasing the concentration of bicarbonate ions, decreasing the availability of carbonate ions and lowering the saturation state of the major shell-forming carbonate minerals. Whereas

(e.g. temperature increase, light availability, nutrient limitation). Potential restructuring of the phytoplankton community (classes, species and cell size; Falkowski et al., 1998; Boyd and Doney, 2002) as a result of ocean acidification will have direct consequences for grazer communities and organic carbon flow. It may also influence the dominance of grazing over other loss processes such as viral lysis, and consequently the cycling of energy and biogeochemically relevant elements, the ratio of production and respiration of the ocean and the efficiency of the biological pump (Brussaard et al., 1996, 2008; Ruardij et al., 2005; Suttle, 2007). Phytoplankton that are consumed by grazers are channeled to higher trophic levels, whereas viral lysis directly forces the food web towards a more regenerative pathway (Brussaard et al., 2005; Suttle, 2007).

OA and other global climate change-related impacts are most striking in both polar regions, where temperatures and acidities are changing at more than twice the global average (Hoegh-Guldberg and Bruno, 2010). The cold Arctic surface waters allow relatively high CO₂ solubility, making this area particularly vulnerable to OA. The present study is part of a collaborative mesocosm CO₂-enrichment experiment performed in Kongsfjorden off Svalbard, summer 2010, within the framework of the European Project on Ocean Acidification (EPOCA). We present here the microbial community dynamics under the influence of elevated *p*CO₂ levels and discuss the consequences for the functioning of the pelagic food web.

2 Material and methods

2.1 Study site and experimental set-up

The study was conducted in Kongsfjorden (78°56'2" N, 11°53'6" E), near Ny-Ålesund, Svalbard, between 31 May and 7 July 2010 (day *t* – 7 to *t*30, where *t*0 is the day after the first CO₂ addition). Nine large mesocosms of approximately 50 m³ (15 m below sea level) were moored in the fjord in sets of 3. The experimental set-up, carbon chemistry dynamics and nutrient concentrations throughout the experiment are described in detail by Riebesell et al. (2013), Bellerby et al. (2013) and Schulz et al. (2013). In short, the mesocosms were filled with fjord water (inorganic nutrient concentrations < 0.1, 0.09, 0.2 and 0.7 μM for nitrate, phosphate, silicate and ammonium, respectively) and screened through a 3 mm mesh to eliminate larger organisms on the 1 of June (*t* – 6). The mesocosms were open to the atmosphere but covered with transparent hoods to minimize input of rain and bird droppings. Two of the mesocosms received no CO₂ addition but were treated otherwise the same, representing the present day carbonate chemistry of the fjord (~ 185 μatm at the start of the experiment). The addition of CO₂ was gradual between day *t* – 1 and *t*4 by pumping CO₂-enriched seawater through a dispersal device which was lowered to about 13 m

depth and gently pulled up several times, resulting in an even distribution throughout the water column. The other 7 mesocosms were enriched with CO₂ over a period of several days (*t* – 1 to *t*4) in varying amounts, resulting in a range of initial *p*CO₂ levels from ~ 270 to ~ 1420 μatm (corresponding to *p*H_T values of 8.18 to 7.51). Two weeks into the experiment (*t*13), inorganic nutrients were added to the originally nutrient-poor water in order to stimulate primary production (5 μM nitrate, 0.3 μM phosphate and 2.5 μM silicate for all mesocosms, to simulate the upwelling of deeper, nutrient-rich water to the nutrient-depleted surface water). The one month experiment showed 4 phases: phase 0 represents the period from closing of the mesocosms to the end of the CO₂ manipulations (*t* – 7 to *t*3), phase 1 corresponds to the period after CO₂ manipulation until the addition of inorganic nutrients (*t*4 to *t*12), phase 2 stands for the period after nutrient addition and until the second chlorophyll minimum (*t*13 to *t*21; Schulz et al., 2013), and phase 3 includes the final period until the end of the experiment (*t*22 to *t*30). Throughout this study the data are presented using 3 colors (blue, grey and red), representing low, intermediate and high *p*CO₂ additions. The low *p*CO₂ addition group contains mesocosms 3, 7 and 2; the intermediate group consists of mesocosms 4, 8 and 1; and the high *p*CO₂ addition group is made up of mesocosms 6, 5 and 9.

Collective sampling was performed daily in the morning using an integrated water sample (0–12 m). From this water subsamples were obtained for counting phytoplankton, heterotrophic prokaryotes (HP) and viruses. Besides this, we sampled 2–3 times per week for the microzooplankton grazing incubations using a gentle vacuum-driven pump system. Samples were protected against daylight by black plastic bags. In the laboratory the samples were maintained and processed (for grazing assay and counting) at in situ temperature and dimmed light. The abundances of phytoplankton were determined on fresh samples. HP and viruses were fixed for 30 min at 7 °C with glutaraldehyde (25 %, EM-grade) at a final concentration of 0.5 % before snap freezing in liquid nitrogen and storage at –80 °C until analysis.

2.2 Microbial abundances

The microbes were enumerated using a bench-top Becton Dickinson FACSCalibur flow cytometer (FCM) equipped with a 488 nm argon laser. The photoautotrophic cells (< 20 μm) were counted fresh and discriminated by their pigment autofluorescence (Marie et al., 1999). Only eukaryotic photosynthetic organisms were detected. Based on their autofluorescence and side scatter signal, the phytoplankton community could be divided into 6 clusters: picophytoplankton I and II, and nanophytoplankton I to IV. Nanophytoplankton III and IV displayed higher side scatter signals than other clusters similar in size. Average cell size of the different clusters was determined by serial gravity filtration of a very small volume of sample (< 10 mL) through different

polycarbonate 47 mm diameter filters (10, 8, 5, 3, 2, 1, 0.8, 0.4 μm) according to Veldhuis and Kraay (2004). Cell sizes of the different clusters ranged between 0.8–2, 2–3, 3–8, 8–10, 5–8 and 3–5 μm diameter for picophytoplankton I, II, and nanophytoplankton I, II, III, and IV, respectively. Assuming the cells to be spherical and containing 0.2 $\text{pg C } \mu\text{m}^{-3}$ (Cuvellier, 2010), cellular carbon was calculated based on the average cell diameters (1.3, 3, 5, 10, 7 and 4 μm , respectively). Estimated cellular carbon contents were 0.18, 2.8, 13.1, 104, 35.8 and 6.7 pg C cell^{-1} for the 6 phytoplankton clusters, respectively (Veldhuis and Kraay, 2004). Net growth and loss rates of phytoplankton were derived from exponential regression analysis of the cell abundances.

The abundances of heterotrophic prokaryotes and viruses were determined from fixed, frozen samples according to Marie et al. (1999) and Brussaard (2004), respectively. In short, thawed samples were diluted with Tris-EDTA buffer (10 mM Tris-HCl and 1 mM EDTA, pH 8) and stained with the green fluorescent nucleic acid-specific dye SYBR-Green I (Molecular Probes, Invitrogen Inc.), for a final concentration of 1×10^{-4} (HP) or 0.5×10^{-4} (viruses) of the commercial stock, in the dark at room temperature for 15 and 10 min, respectively. HP and viruses were discriminated in bivariate scatter plots of green fluorescence versus side scatter. Final counts were corrected for a blank consisting of TE-buffer and SYBR-Green I prepared and analysed in an identical manner to the samples. Two HP clusters (HDNA – high DNA fluorescent – and LDNA – low DNA fluorescent) and 5 viral groups (V1–V5) were distinguished.

2.3 Microzooplankton grazing

Microzooplankton grazing of phytoplankton was determined using the dilution method of Landry and Hassett (1982). In short, whole seawater samples were sieved through a 200 μm mesh to remove mesozooplankton, after which the sample was combined with 0.45 μm filtered seawater (0.45 μm Sartopore capsule filter, containing a 0.8 μm pre-filter) over a dilution series of 20, 40, 70 and 100 % to create a gradient in microzooplankton grazing pressure. All treatments were set up in triplicate in clear 1.2 L polycarbonate bottles. The bottles were incubated at in situ temperature and natural light. Subsamples were taken at 0 and 24 h, and phytoplankton abundance was enumerated immediately by FCM. Phytoplankton growth rates were plotted against the level of dilution, and model 1 regression analysis was performed to obtain the actual microzooplankton grazing rate (slope) and apparent phytoplankton growth rate in the absence of grazing (intercept y-axis). All seawater handling was performed at in situ temperature and under dim light conditions using Nitrile gloves. For logistical reasons we could only handle two dilution assays at a time. We choose to sample mesocosm 3, representing present time $p\text{CO}_2$ level, as reference for mesocosm 8 (intermediate $p\text{CO}_2$ levels) and mesocosm 5 (high $p\text{CO}_2$ levels), which each were sampled alternately. Microzooplank-

ton grazing on nanophytoplankton II–IV failed due to the low whole water abundances ($<200 \text{ mL}^{-1}$).

2.4 Statistics

For the statistical tests we used SYSTAT version 13.00.05 (SYSTAT Software, Inc. 2009, San Jose, CA). The hypothesis that there was no difference in growth rates of microbes in diverse time frames during the mesocosm experiment was tested using one-way ANOVA. Testing overall differences in standing stock of diverse flow cytometric clusters during different time periods was performed using ANOVA with the square root-transformed abundances as the dependent variable, mesocosm as factor, and the sampling day as covariate. To test the specified hypothesis, contrasts in the post hoc hypothesis tests were used. The grazing rates were calculated in Excel, including the standard error of the grazing rates (i.e. standard error of the estimated slope of the regression line). *P* values indicate if the grazing rates differ significantly from zero.

3 Results

3.1 Phytoplankton abundances and net growth

The abundance of each phytoplankton cluster is presented in Fig. 1. Total phytoplankton abundance was strongly dominated by picophytoplankton I (Fig. 1a), generally making up more than 90 % of the total count, except for $t1$ to $t11$ when their share declined to 60 % due to a bloom of nanophytoplankton (Fig. 1c). Picophytoplankton I showed a steady increase until $t18$, after which the bloom declined sharply (Fig. 1a). The net growth rates during phase 1, derived from the standing stock and calculated using the natural logarithm, were on average 0.14 ± 0.03 , 0.15 ± 0.03 and 0.17 ± 0.02 for the low, intermediate and high $p\text{CO}_2$ mesocosms, respectively. During phase 2, after inorganic nutrient addition, the net growth rates of the picophytoplankton I were slightly higher, ranging from 0.14 to 0.24 d^{-1} (no significant correlation with $p\text{CO}_2$, however). Highest net peak abundances, i.e. $1.1\text{--}1.5 \times 10^5 \text{ cells mL}^{-1}$, were recorded for the high $p\text{CO}_2$ mesocosms 5, 6, and 9 (ANOVA, $p < 0.000$). Picophytoplankton II increased until $t7$ at a net growth rate between 0.30 and 0.38 d^{-1} (Fig. 1b). The highest abundances of $3.5\text{--}4.9 \times 10^3 \text{ cells mL}^{-1}$ during phase 1 were observed for the intermediate and low $p\text{CO}_2$ mesocosms (ANOVA, $p < 0.000$).

Nanophytoplankton I increased steeply from the start of the experiment, growing at net growth rates between 0.51 and 0.55 d^{-1} (with the exception of mesocosm 4 showing a growth rate of 0.42 d^{-1}), and peaked at $t4\text{--}6$ with maximum abundances between 1.6 and $1.8 \times 10^3 \text{ cells mL}^{-1}$ (Fig. 1c). A second increase was found during the last week of the experiment with highest abundances typically in the higher $p\text{CO}_2$ mesocosms. Nanophytoplankton II were present in

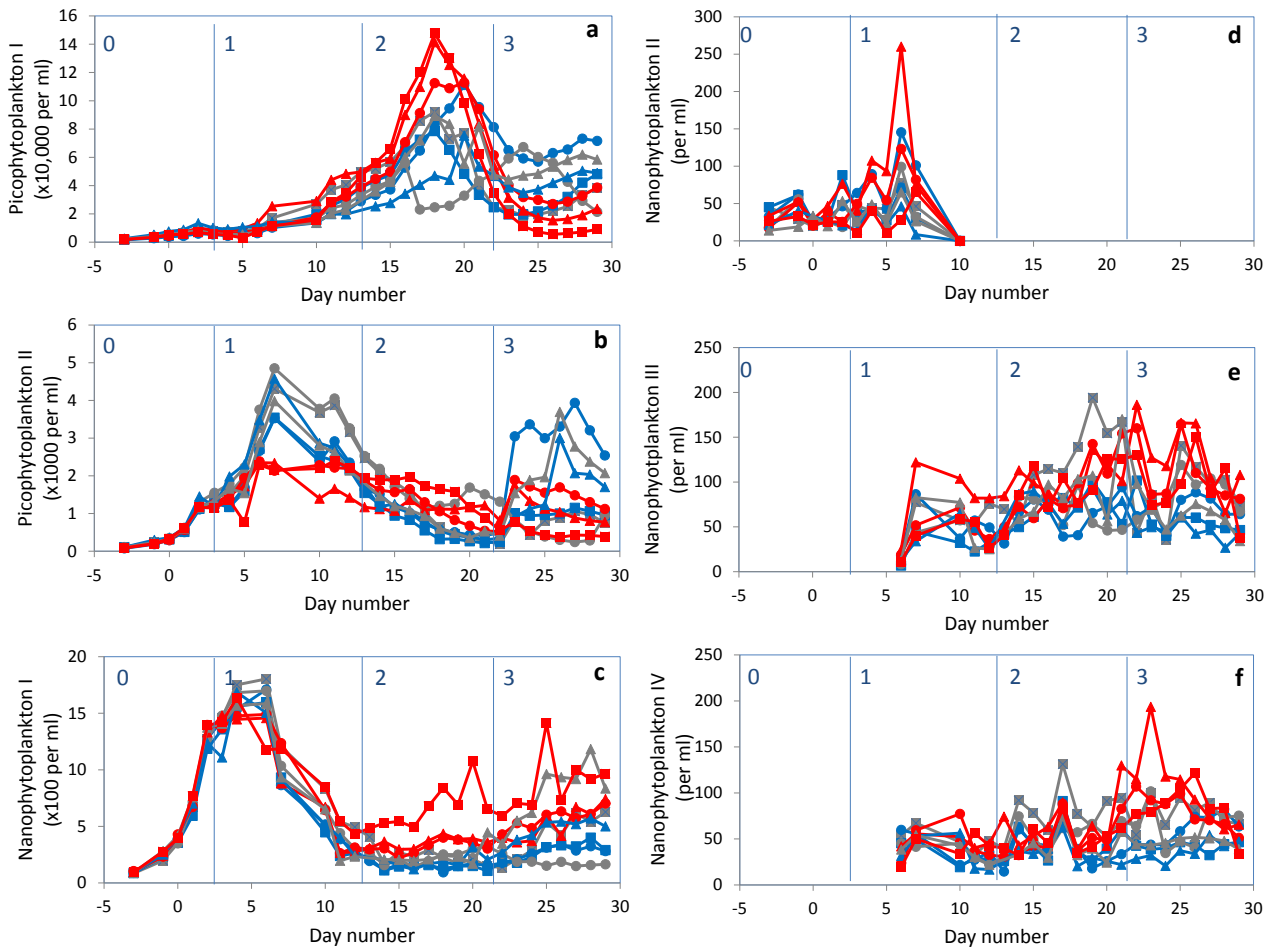


Fig. 1. Temporal dynamics of depth-integrated (0.3–12 m) picophytoplankton cluster I (a), picophytoplankton cluster II (b), nanophytoplankton I (c), nanophytoplankton II (d), nanophytoplankton III (e) and nanophytoplankton IV (f). Only eukaryotic photosynthetic organisms were detected. Low CO_2 treatments are blue, intermediate CO_2 treatments are grey, and high CO_2 treatments are red colored. In order of low, intermediate and high $p\text{CO}_2$ mesocosms, the circles represent mesocosms M3, M4 and M6; triangles M7, M8 and M5; and squares M2, M1 and M9, respectively.

low numbers (generally below $150 \text{ cells mL}^{-1}$) and could no longer be detected in either the mesocosms or the natural fjord water from t_{10} onwards (Fig. 1d). Around the same time (t_6), a new phytoplankton population, nanophytoplankton III, appeared that was undetectable until then (Fig. 1e). It remained present throughout the duration of the experiment at a rather stable concentration ($<150 \text{ cells mL}^{-1}$), with significantly higher algal numbers for the high $p\text{CO}_2$ mesocosms during phase 2 and 3 (ANOVA, $p < 0.000$). Nanophytoplankton IV showed similar algal concentrations, with significantly higher abundances during phase 3 in the high $p\text{CO}_2$ addition mesocosms (Fig. 1f; ANOVA, $p < 0.000$).

Figure 2 shows the phytoplankton ($<20 \mu\text{m}$) cellular carbon (algal POC). The first maximum at t_5 is due to the peak in nanophytoplankton around that time (Fig. 2a). Despite their relatively low numbers, their larger size results in algal POC concentrations similar to or higher than that of the

more abundant (up to 70-fold higher cell abundances) but very small picoeukaryotic algae that are responsible for the second maximum of algal POC (Fig. 2b).

3.2 $p\text{CO}_2$ -related phytoplankton trends

As expected, all mesocosms resembled each other for microbial abundances during the initial phase 0 ($t = -7$ to t_3). Shortly after completing CO_2 additions (at t_7 ; phase 1), the standing stock of picophytoplankton II in the three high $p\text{CO}_2$ mesocosms, 5, 6 and 9, showed a negative response (Fig. 3a). This response was, however, not maintained and even reversed after nutrients were added at t_{13} . It has to be noted that picophytoplankton II was made up by 3 subpopulations that were hard to separate. A weak positive correlation with $p\text{CO}_2$ during phase 1, thus prior to nutrient addition, was only observed for picophytoplankton I ($y = 16.6x + 20\,963$, $r^2 = 0.516$). Upon the addition of inorganic nutrients (phase 2),

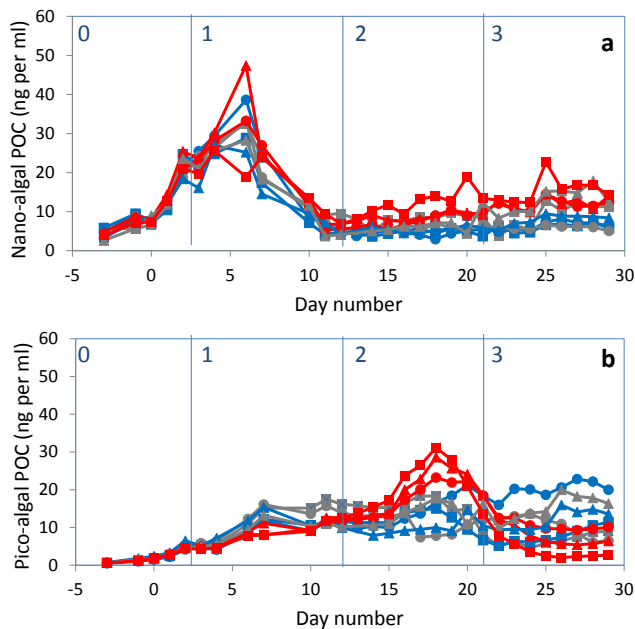


Fig. 2. Temporal development of algal particulate organic carbon (POC) for total nanophytoplankton ((a) Nano-algal POC) and picophytoplankton ((b); Pico-algal POC). For color and symbol coding, see Fig. 1.

picophytoplankton II became dominated by one of those sub-populations. Interestingly, the peak abundances of picophytoplankton I at $t18$ correlated strongly and positively with $p\text{CO}_2$ (Fig. 3b). Net growth rates until $t18$ were on average $0.15\text{--}0.20\text{ d}^{-1}$ (no significant trend with $p\text{CO}_2$ observed). However, a statistically significant and positive relationship with $p\text{CO}_2$ was found for the cell abundances of picophytoplankton II and nanophytoplankton I (Fig. 3c and d; $p = 0.008$). Nanophytoplankton III and IV furthermore showed positive correlations with $p\text{CO}_2$ only until $600\ \mu\text{atm}$ (r^2 of 0.903 and 0.610, respectively), however, the low cell abundances ($<150\ \text{mL}^{-1}$) caution for over-interpretation (higher statistical error). Notwithstanding, the positive correlation between phytoplankton standing stock and $p\text{CO}_2$ levels at $t18$ is clearly illustrated by total algal POC (Fig. 4).

Within phase 1 of the experiment ($t4$ to $t13$), the net loss rates during the decline of the nanophytoplankton I peak ($t6$ to $t13$) were negatively correlated with $p\text{CO}_2$, i.e. lower net loss rates at higher $p\text{CO}_2$ levels (from -0.15 d^{-1} at high $p\text{CO}_2$ to -0.3 d^{-1} at low $p\text{CO}_2$; Fig. 5a). During the decline of the picophytoplankton II bloom ($t7$ to $t22$) the highest $p\text{CO}_2$ mesocosms also showed reduced net loss rates (on average $-0.10 \pm 0.04\text{ d}^{-1}$ as compared to $-0.19 \pm 0.03\text{ d}^{-1}$ for the other mesocosms; Fig. 5b). In contrast, the net loss rates after the bloom of picophytoplankton I ($t18\text{--}26$) show a positive correlation with $p\text{CO}_2$ when excluding mesocosm 4, which had already declined before that period (on average $-0.32 \pm 0.1\text{ d}^{-1}$ for the mesocosms with $p\text{CO}_2 \geq 600\ \mu\text{atm}$

and $-0.19 \pm 0.07\text{ d}^{-1}$ for $p\text{CO}_2 \leq 600\ \mu\text{atm}$; Fig. 5c). At the end of the experiment ($t27$), the picophytoplankton I show a negative correlation with $p\text{CO}_2$, however, we argue below that at this stage into the experiment such a correlation is the indirect effect of viral lysis and grazing dynamics.

3.3 Phytoplankton viruses and microzooplankton grazing

The viral community could be discriminated into 5 distinct clusters, of which two (V4 and V5) are considered most likely algal viruses (Fig. 6; Brussaard and Martínez Martínez, 2008). The abundance of viruses V4 started to increase upon the development of the nanophytoplankton I bloom and showed its strongest increase concomitantly with the decline of this phytoplankton group (Figs. 1c and 6a). Moreover, V5 increased sharply the moment the bloom of picophytoplankton I declined ($t18$; Figs. 1a and 6b), indicating a regulating role of viruses on the dynamics of also this phytoplankton population.

Microzooplankton grazing rates (Table 1) showed high grazing on picophytoplankton I during the first days of the experiment (phase 0; around $0.45 \pm 0.14\text{ d}^{-1}$). Grazing rates dropped after phase 0 down to $0.1\text{--}0.2\text{ d}^{-1}$. No correlation with $p\text{CO}_2$ was observed. For unknown reasons, the dilution assay during the first half of the experiment (phase 0 and 1) did not provide good grazing data for the picophytoplankton II. During the second half of the experiment (phase 2 and 3), grazing on picophytoplankton II was substantial (on average $0.39 \pm 0.30\text{ d}^{-1}$), and although grazing rates seem somewhat higher at high $p\text{CO}_2$, the low number of grazing experiments does not validate a statistically significant conclusion. Microzooplankton grazing on nanophytoplankton I was on average $0.44 \pm 0.36\text{ d}^{-1}$ throughout the experiment, with high rates during phase 2 ($0.81 \pm 0.26\text{ d}^{-1}$ vs. $0.28 \pm 0.40\text{ d}^{-1}$ for other phases).

3.4 HP and viral dynamics

The abundance of HP in all mesocosms dropped abruptly during the first week (by $1.5 \times 10^6\ \text{mL}^{-1}$; Fig. 7a), which was fully due to the decline in the high nucleic acid (HDNA) HP population. The % HDNA HP dropped from around 80 to 40–55 % at $t7$ (Fig. 7b). Viruses increased in abundance around $1 \times 10^7\ \text{mL}^{-1}$ (Fig. 8a). The concomitant decline of HP and increase in viruses resulted in a steeply increasing total virus to prokaryote ratio (VPR), from 25 up to 150 (Fig. 8b). After $t7$ the total HP community increased steadily again (Fig. 7a). The % HDNA HP also increased again up to a maximum of 70 % at $t14$ (Fig. 7b), after which it decreased steadily, resulting in an equal contribution of HDNA and LDNA HP towards the end of the experiment (phase 3). HP net growth rates, derived from $t5$ to the end of the experiment, correlated negatively to $p\text{CO}_2$, which consequently resulted in a negative correlation between HP abundance at $t28$

Table 1. Microzooplankton grazing rates on phytoplankton (d^{-1}) for 3 mesocosms representing low, intermediate (mid) and high pCO_2 levels. Mesocosm M3 (low, i.e. present time pCO_2) was sampled as reference to mesocosm M5 and M8. Failed assays for specific phytoplankton clusters are indicated by –. Standard error between parentheses. Statistical significance indicated by * $p = 0.1–0.05$; ** $p = 0.05–0.01$; *** $p = 0.01–0.001$; and **** $p = 0.001–0$.

Mesocosms (pCO_2)	Picophytoplankton I			Picophytoplankton II			Nanophytoplankton I		
	Low 3	Mid 8	High 5	Low 3	Mid 8	High 5	Low 3	Mid 8	High 5
1	0.62 (0.15)*	0.37 (0.15)	–	–	–	–	0.30 (0.10)**	0.04 (0.06)	–
3	0.50 (0.09)****	0.31 (0.07)***	–	–	–	–	0.04 (0.10)	–	–
7	0.09 (0.14)	–	0 (0.07)	–	–	0.01 (0.09)	0.35 (0.14)**	–	0.20 (0.15)
12	–	0.10 (0.05)*	–	–	0.01 (0.07)	–	0.39 (0.21)*	0.48 (0.26)*	–
16	0.02 (0.03)	0.05 (0.05)	–	–	–	–	1.29 (0.24)****	0.58 (0.30)*	–
20	0.04 (0.03)	–	0.15 (0.05)**	0.39 (0.12)**	–	0.98 (0.31)**	0.65 (0.19)****	–	0.65 (0.19)***
22	–	0.12 (0.04)**	–	0.04 (0.24)	0.78 (0.07)***	–	0.88 (0.24)***	0.78 (0.23)***	–
24	0 (0.03)	–	0.17 (0.03)****	0.01 (0.23)	–	0.41 (0.11)***	0.34 (0.17)*	–	0.40 (0.10)***
26	0.19 (0.06)*	0.09 (0.03)***	–	0.36 (0.06)****	0.37 (0.07)***	–	0.66 (0.23)**	0.40 (0.15)**	–
28	0.01 (0.05)	–	0.18 (0.04)****	0.31 (0.07)***	–	0.29 (0.01)**	0.30 (0.20)	–	0.51 (0.28)*

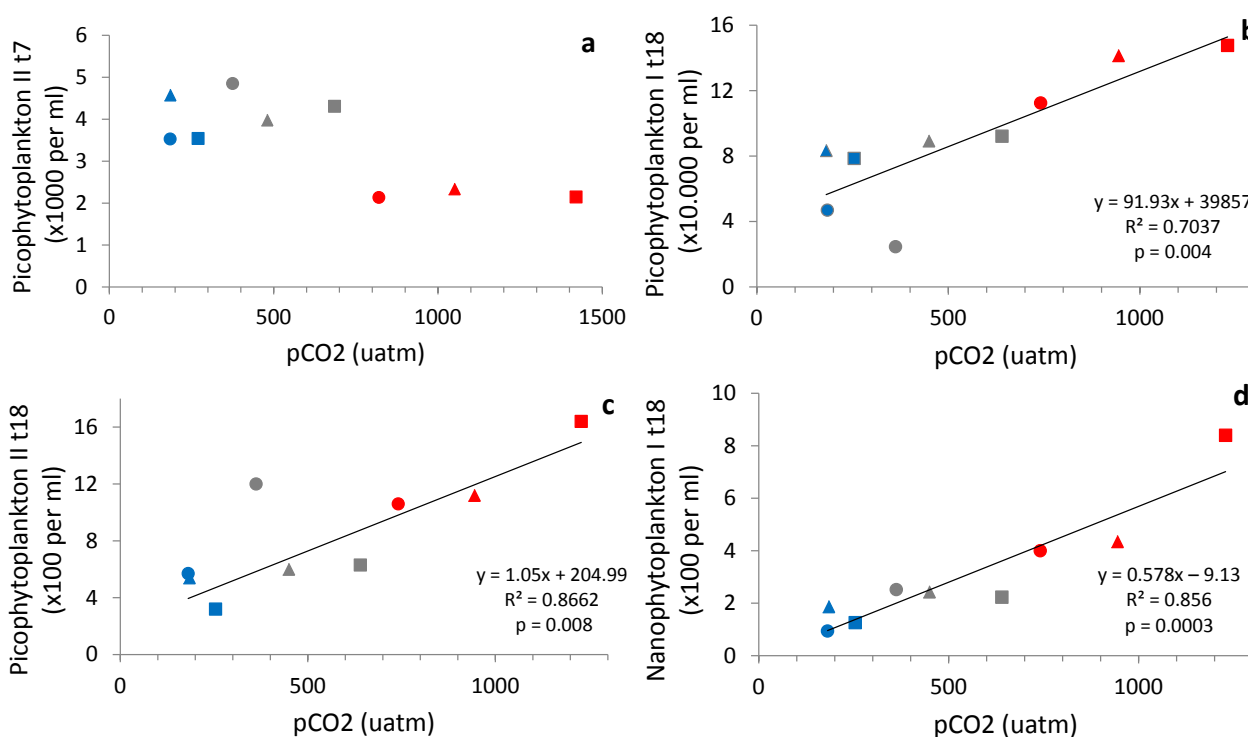


Fig. 3. Phytoplankton cell abundance versus actual pCO_2 for picophytoplankton II on $t7$ (a), picophytoplankton I on $t18$ (b), picophytoplankton II on $t18$ (c), and nanophytoplankton I on $t18$ (d). For (b–d) the CO_2 concentrations plotted were the averages of $t8$ to $t18$. For color and symbol coding, see Fig. 1. Linear regression statistics provided in plots.

and pCO_2 levels (Fig. 7c). No such trend was found for virus abundances. However, the slopes of the linear regression of viruses versus HP per mesocosm plotted against pCO_2 levels resulted in a linear correlation (Fig. 8c), which suggests a stronger impact of viruses on HP dynamics at higher pCO_2 .

4 Discussion

The Arctic Ocean ecosystem is particularly vulnerable to OA related alterations due to the relatively high CO_2 solubility and low carbonate saturation states of its cold surface waters. Thus far, however, there is only little known about the consequences of OA on the base of the food web. In a mesocosm CO_2 -enrichment experiment (overall CO_2 levels ranged from ~ 180 to $1100 \mu atm$) in Kongsfjorden off Svalbard, we studied the consequences of OA on a natural pelagic microbial

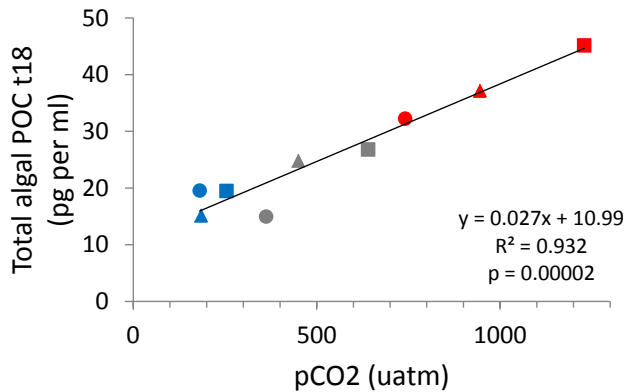


Fig. 4. Total algal POC versus $p\text{CO}_2$. The CO_2 concentrations plotted were the averages of $t8$ to $t18$. For color and symbol coding, see Fig. 1. Linear regression statistics provided in plots.

community. Overall, our results show that elevated CO_2 stimulated the growth of the smallest size range of primary producers, thereby substantially affecting the structure and functioning of the pelagic food web in the future.

4.1 Phase 0

The initial phase of the experiment showed an increase in standing stock of the phytoplankton clusters picophytoplankton II (2–3 μm diameter) and nanophytoplankton I (3–8 μm diameter). For nanophytoplankton I the gross growth rate based on the net growth rates and grazing rate (dominant loss factor) compares well with the 0.87 d^{-1} gross growth rate obtained by ^{13}C -uptake for a phytoplankton group that included nanophytoplankton (De Kluijver et al., 2013). Inorganic nutrients were depleted due to the spring bloom preceding our experiment, and thus, the smaller-sized phytoplankton had a competitive advantage by growing on remineralised ammonia and inorganic phosphate (Schulz et al., 2013). Furthermore, utilization of organic nutrients and mixotrophy may also have allowed growth by these phytoplankton groups (Schulz et al., 2013). Light microscopy data showed that nano-sized (around 5 μm cell diameter, thus potentially belonging to nanophytoplankton I) *Pseudopedinella* sp., a known mixotroph, peaked around $t4$ (A. Stühr, personal communication, 2012). Another mixotroph chrysophyte, i.e. *Ochromonas* sp., also developed during phase 0 and into phase 1 (A. Stühr, personal communication, 2012). However, expressed in organic carbon, these chrysophytes were not the dominant nanoeukaryotes. Phytoplankton pigment analysis showed dominance of Prasinophyceae and Haptophyceae (Schulz et al., 2013), which are known to consist largely of pico- and nanophytoplankton, respectively. Members of Prasinophyceae have been found to be the most abundant picophytoplankton (Zhu et al., 2005), although recently Cuvellier et al. (2010) found that picopyrnesiophytes (Haptophyceae) may also contribute to global picophytoplankton

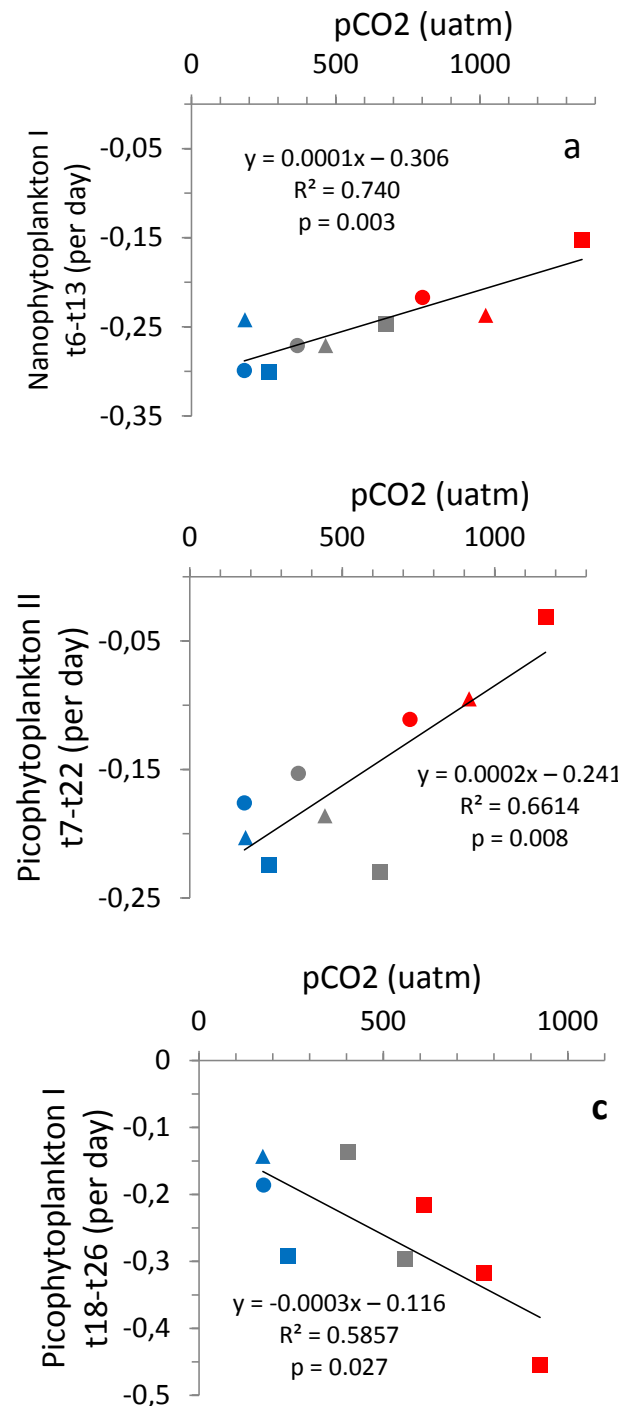


Fig. 5. Specific growth rates determined from the net phytoplankton abundances versus $p\text{CO}_2$. Nanophytoplankton I from $t6$ – $t13$ (a), picophytoplankton II from $t7$ to $t22$ (b), and picophytoplankton I from $t18$ – $t26$ (c). A negative growth rate indicates cell loss. The CO_2 concentrations plotted were the averages for the specific time periods indicated. For color and symbol coding, see Fig. 1. Linear regression statistics provided in plots.

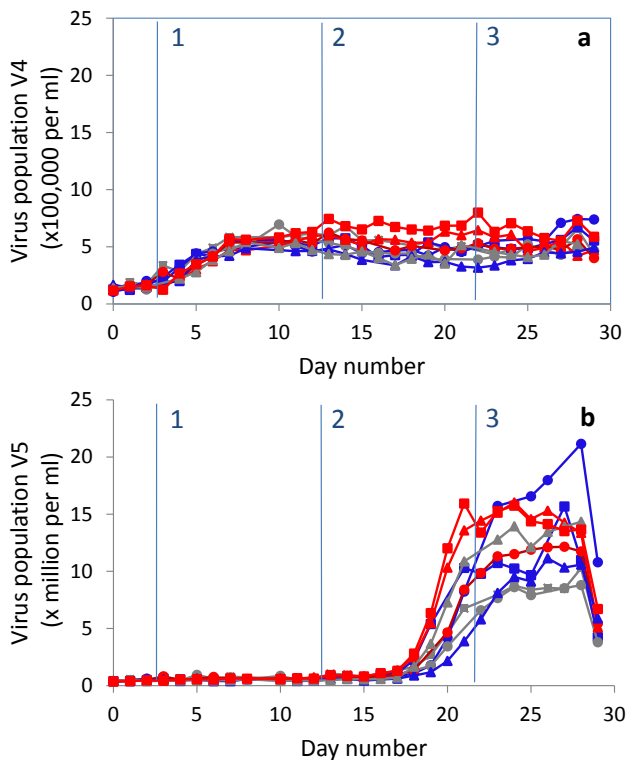


Fig. 6. Temporal dynamics of virus cluster V4, indicative of larger algal viruses infecting nanophytoplankton I (a), and V5, most likely infecting picophytoplankton I (b). For color and symbol coding, see Fig. 1. Note the different y-axis scales.

biomass. Recently, dominance of picophytoplankton has also been shown in the perennially cold ocean in the Canadian Arctic during summer (>70 % of total cell count; Tremblay et al., 2009). Additionally, some diatoms were still present, but these were typically larger than detectable by the flow cytometer used in this study (Schulz et al., 2013).

We noted a clear decline in the HP standing stock during the period of CO₂ manipulations (of 0.2×10^5 HP mL⁻¹ d⁻¹) that matched the decline in HP production (Motegi et al., 2013) and was likely due to viral lysis. Virus-mediated mortality rates were higher than throughout the rest of the experiment, i.e. 90 % of standing stock lysed d⁻¹ vs. 23 % d⁻¹, whereas grazing by heterotrophic nanoflagellates accounted for about one third of the mortality of the standing stock (W. Weinbauer, personal communication, 2012). The estimated burst size was on average 7 viruses per lysed bacterium cell (estimated from the net loss of HP and net production of viruses), which may seem somewhat low (see review by Parada et al., 2006), but Middelboe et al. (2002) have observed similar burst sizes in Arctic water during summer and Boras et al. (2010) have reported a burst size of 1–59 viruses per bacterium in north Svalbard during summer. Interestingly, specifically the HDNA HP were affected. Phage proliferation has been

found to depend on host metabolism (e.g. HP host generation times; see review by Weinbauer, 2004), and HDNA HP have been reported to represent the metabolically active members of the microbial community (Lebaron et al., 2001). However, some contrasting studies did show that LDNA HP can also be an active part of the microbial population (Zubkov et al., 2001; Brussaard et al., 2005; Wang et al., 2009). Preferential grazing on HDNA HP has been implied (Gasol et al., 1999; Vaqué, 2001), although cell size instead of metabolic activity might have been the underlying reason. Still, the selective loss of HDNA HP due to viral lysis has not been, to our knowledge, yet reported.

4.2 Phase 1

This phase is the only period in which the sole effect of the CO₂ treatment could be determined as nutrients were not added yet (*t*13). Phase 1 was dominated in algal POC by nanophytoplankton, peaking around *t*5. The study by Schulz et al. (2013) showed that the Haptophyceae was the principal algal class. Although no obvious correlation between the peak abundances and *p*CO₂ was recorded, we did find a significant negative correlation of the net loss rates (obtained from the decline in net abundances) with *p*CO₂. The relatively high net loss rates for nanophytoplankton I in the low CO₂ mesocosms (0.30 d⁻¹ as compared to 0.20 d⁻¹ for the high CO₂ mesocosms) corresponded well with the higher microzooplankton grazing rates found at the low CO₂ level (0.35 d⁻¹ vs. 0.20 d⁻¹ at high *p*CO₂). OA has been reported not to affect microzooplankton abundance or grazing activity (Suffrian et al., 2008), however in contrast to our study, neither phytoplankton composition nor succession differed between their CO₂ treatments (Riebesell et al., 2007). Still, OA during the present study did not significantly affect the diversity of the protozooplankton (ciliates and heterotrophic dinoflagellates), indicating to a high tolerance of this Arctic protozooplankton community to changes in *p*CO₂/pH (Aberle et al., 2013). Although grazing on nanophytoplankton I matched the net loss rates, viral lysis also accounted for substantial loss (based on increase of virus V4 and concurrent decline of nanophytoplankton I), which implies that the nanophytoplankton still grew but that the higher loss rates resulted in the decline of the algal bloom. De Kluijver et al. (2013) indeed still recorded ¹³C utilization by the nanophytoplankton during *t*5 to *t*10.

Assuming half the net decline in nanophytoplankton I abundance to be due to viral lysis, we found viral burst sizes (i.e. the number of newly produced viruses released per lysing host cell; derived from the net increase in V4 abundance and half of the net decline in algal host abundance) of 540–764 for the different mesocosms. The literature shows comparable burst sizes for nanophytoplankton host-virus model systems from the Haptophyceae class, e.g. 350–600 for *Phaeocystis globosa* and *P. pouchetii* and

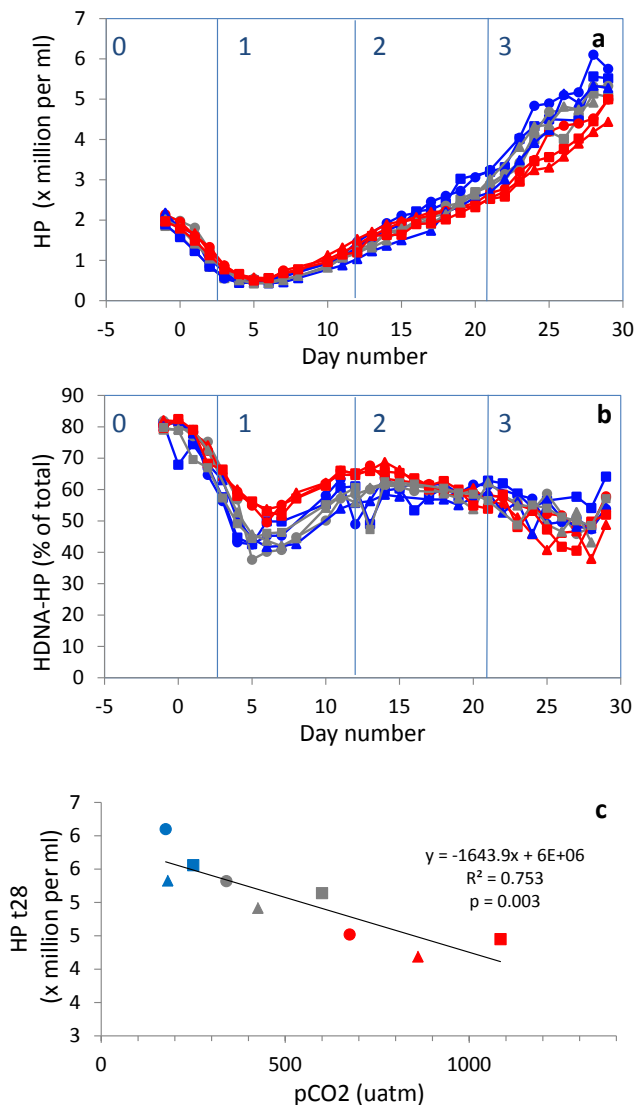


Fig. 7. Temporal development of heterotrophic prokaryotes HP (a) and HDNA HP (b). The abundance of HP at t_{28} versus $p\text{CO}_2$ (average of t_8 to t_{27}) is plotted in (c). For color and symbol coding, see Fig. 1. For (c), the linear regression statistics are provided in plot.

400–1000 for *Emiliania huxleyi* (see review by Brussaard and Martínez Martínez, 2008).

The utilization of the organic matter released by viral lysis of the HP (phase 0) and the nanophytoplankton (phase 1) resulted in a steady increase in HP abundance after t_5 . Based on half of the nanophytoplankton lost due to viral lysis, a HP carbon conversion of $12 \text{ fg C cell}^{-1}$ (Fukuda et al., 1998), a HP growth efficiency of 30 % (Motegi et al., 2013) and taking 50 % mortality of the heterotrophic HP into account (Motegi et al., 2013), we estimated that the cellular carbon released by viral lysis (about $30 \mu\text{g C L}^{-1}$) sustained about a third of the gross HP carbon demand during phase 2. Extracellular enzyme activities and bacterial protein production indeed in-

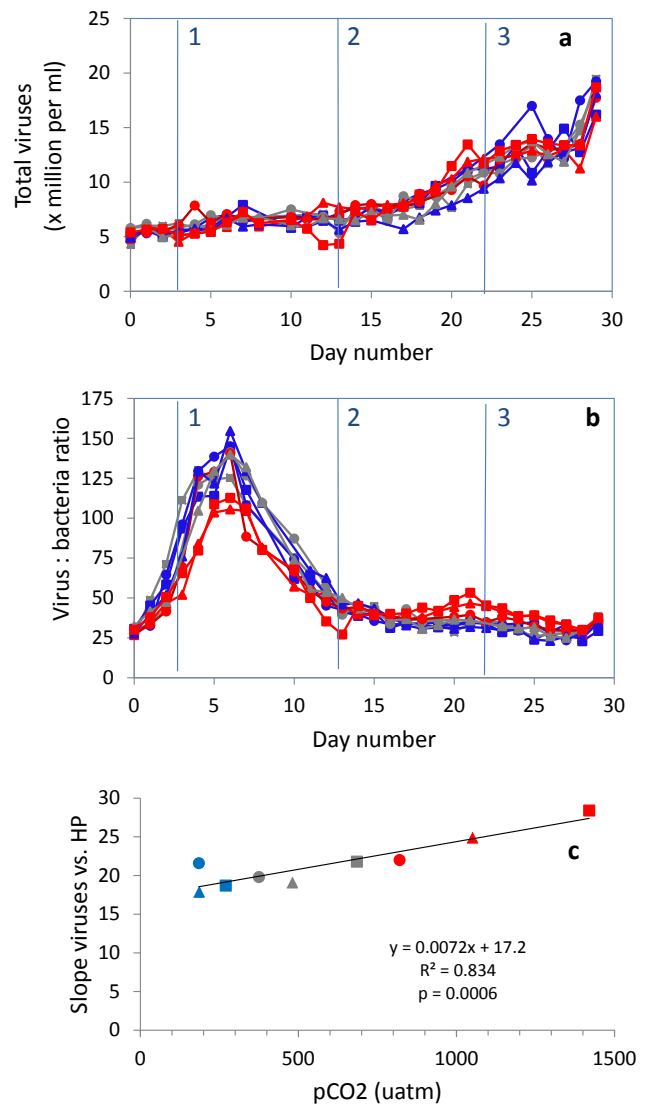


Fig. 8. Temporal dynamics of total viruses (a) and the virus to HP ratio (b). Furthermore, the slope of viruses versus HP, thus representing the average number of viruses per HP, for each mesocosm is plotted versus the concurrent $p\text{CO}_2$ (averaged over t_8 to t_{27}) in (c). For color and symbol coding, see Fig. 1. For (c), the linear regression statistics are provided in plot.

creased already during phase 0 and peaked during t_5 to t_{10} (Piontek et al., 2013), concomitantly with the virally induced decline in nanophytoplankton I.

The abundance of picophytoplankton II peaked at t_7 but was significantly (ANOVA $p < 0.000$) lower for the high CO_2 mesocosms (~ 650 – $1100 \mu\text{atm}$). It is unclear whether these algae became negatively affected in their growth at the higher future CO_2 levels or the loss rates for the high $p\text{CO}_2$ mesocosms were enhanced (grazing estimates on picophytoplankton II during this phase failed for the low $p\text{CO}_2$ mesocosm). Hopkins et al. (2010) reported a similar finding for a mesocosm experiment in a fjord in Norway, showing lower

abundances of large picophytoplankton under high $p\text{CO}_2$ (750 μatm) than in the present day CO_2 enclosure. Still, picophytoplankton II formed a complex cluster with 2–3 subpopulations that could not be separated from each other. A shift to one subpopulation in response to elevated $p\text{CO}_2$ may also have been responsible for the obtained results.

During phase 1 the abundances of the small-sized picophytoplankton I (average 1.2 μm cell diameter) increased steadily at $0.15 \pm 0.03 \text{ d}^{-1}$ (not significantly different from each other). Correcting for grazing loss, the gross growth rates were overall 0.1 d^{-1} higher. Already prior to nutrient addition, a weak positive correlation between abundance and $p\text{CO}_2$ emerged, suggesting that elevated CO_2 stimulated the growth of these very small-sized phytoplankton (0.8–2 μm). The trend developed strongly into phase 2 (see Sect. 4.3), emphasizing that elevated CO_2 stimulates growth and nutrient utilization (Schulz et al., 2013) leading to enhanced production of the smallest size range of primary producers.

4.3 Phase 2

Phase 2 represents the initial period upon the addition of inorganic nutrients, allowing for potential growth of larger-sized phytoplankton. Elevated CO_2 in combination with nutrient addition stimulated the growth of the smaller-sized phytoplankton, as shown by the positive correlation of algal POC at $t18$ with $p\text{CO}_2$. These results were supported by the higher uptake rates of the added inorganic nutrients for the highest $p\text{CO}_2$ mesocosms (Schulz et al., 2013). Interestingly, the prevailing group of algae during this period was still the picophytoplankton (particularly cluster I) and to a lesser extent the nanophytoplankton. Algal pigment analysis and light microscopic screening indicated that Prasinophyceae was the dominant algal class, and larger-sized phytoplankton like diatoms were largely absent still (Schulz et al., 2013).

Our results clearly show that the very small-sized picophytoplankton became dominant under increased CO_2 levels, indicating that this group does not or still inefficiently applies carbon concentrating mechanisms (CCMs). Diffusion of CO_2 is typically not expected to limit photosynthesis in the very small-sized phytoplankton (Giordano et al., 2005), although CCMs were identified for the picophytoplankter *Micromonas pusilla* (Worden et al., 2009). Yet, despite their small size (and thus large surface to volume ratio) their diffusive CO_2 uptake seems insufficient and their CO_2 sensitive photosynthesis benefitted from elevated $p\text{CO}_2$. Only a small response to OA (e.g. 10%; The Royal Society, 2005 and references therein) can still result in dominance over time under the assumptions that the loss factors (grazing, viral lysis) do not show direct responses to elevated $p\text{CO}_2$ and other growth variables are not limiting the growth. We found no evidence that grazing or viral lysis rates were directly affected by elevated CO_2 levels, and nutrients and irradiance were non-limiting at the time. The higher abundances of picophytoplankton I at high $p\text{CO}_2$ re-

sulted thus from somewhat enhanced growth rates. Paulino et al. (2008) reported an increased abundance of picophytoplankton in a high CO_2 mesocosm; however, this was towards the end of the experiment when all nutrients were depleted. During another Norwegian fjord mesocosm experiment, still nutrient-replete, the total number of small-sized picophytoplankton did not change under increased $p\text{CO}_2$ (750 μatm ; Hopkins et al., 2010; Newbold et al., 2012). The abundances based on quantitative PCR of specifically the picophytoplankter *Micromonas pusilla*, nevertheless, enhanced significantly (Meakin and Wyman, 2011). A similar trend was observed a few years earlier at the same location, time of the year and experimental set-up, this time based on a *M. pusilla*-like flow cytometric signature (Engel et al., 2008). Meakin and Wyman (2011) showed that the picophytoplankter *Bathycoccus* (also belonging to the Prasinophyceae) was not affected by the increased CO_2 concentrations. Although we have no knowledge of the actual species that are represented by our flow cytometric clusters, our data show (1) the dominance of the picoeukaryotic phytoplankton in polar waters and (2) the potential ecological importance this group will have in future oceans.

High grazing pressure kept the abundances of nanophytoplankton I under control during phase 2 (on average $0.81 \pm 0.26 \text{ d}^{-1}$). Our data suggest that grazing was not affected by $p\text{CO}_2$ (a relationship with $p\text{CO}_2$ could not be tested for shortage of grazing rates in the high CO_2 mesocosms) and viral lysis was not a substantial loss factor at the time, implying that the higher standing stock of the nanophytoplankton I under elevated CO_2 was also due to higher growth rates (as for the picophytoplankton I).

For the picoeukaryotes I viral lysis was the dominant loss factor ($0.2\text{--}0.3 \text{ d}^{-1}$ while grazing $<0.1 \text{ d}^{-1}$), with the steepest increase of virus population V observed for the highest $p\text{CO}_2$ mesocosms (in agreement with the strongest decline of picophytoplankton I at these CO_2 levels). Estimated burst sizes ranged between 119 and 245 (derived from the net increase in $V5$ abundance and net decline in algal host abundance), matching the published values for prasinophyte picophytoplankton host-virus model systems (e.g. 72–360 for *Micromonas pusilla*; Waters and Chan, 1982; Baudoux et al., 2008). The resultant release of cellular organic carbon due to viral lysis of the picophytoplankton I increased with CO_2 level, i.e. 7, 10 and 20 $\mu\text{g C L}^{-1}$ for the low, intermediate and high $p\text{CO}_2$ mesocosms. Based on the HP net growth rate of $0.2 \times 10^5 \text{ cells mL}^{-1} \text{ d}^{-1}$, a growth efficiency of 30% and low mortality (Moteqi et al., 2013), viral lysis accounted for 15 to 42% of the gross HPC demand.

4.4 Phase 3

Despite the enhanced release of the lysing algal cells in the highest $p\text{CO}_2$ mesocosms that continued into phase 3, the HP standing stock was significantly lower at elevated CO_2 (ANOVA, $p < 0.000$). We speculate that this may have been

due to higher viral lysis rates as a result of higher VPR and therefore encounter rate.

During this last phase of the experiment, picophytoplankton were still most abundant but the biomass share of the nanophytoplankton became more important, equaling picophytoplankton. Schulz et al. (2013) showed that the Haptophyceae, containing many nanoeukaryotic phytoplankton species, increased in abundance during this phase. The same authors showed, furthermore, that larger-sized photoautotrophs such as the Dinophyceae became an important group and were positively correlated to elevated CO₂. In contrast, the growth of diatoms and Chlorophyceae was reduced at elevated CO₂, most likely due to diminished nutrient availability (inorganic nutrients became depleted during the second half of Phase 3). Species in these phytoplankton classes often have efficient CCMs that allow for optimal photosynthesis and growth at ambient (and past) CO₂ concentrations and, therefore, are not (or only minimally) affected by increased CO₂ levels (Giordano et al., 2005; Engel et al., 2008; Rost et al., 2008).

5 Conclusions

The most prominent finding of our study is the evident impact of OA on the composition and growth of the Arctic phytoplankton community, i.e. the picoeukaryotic photoautotrophs and to a lesser extent the nanophytoplankton prospered. This mesocosm experiment took into account at least 4 of the 7 future research recommendations stated by Rost et al. (2008), namely it mimicked the environmental conditions as closely as possible, was community based (microbial food web), involved the interactive effects of multiple environmental variables in combination with CO₂, and tried to unravel the underlying mechanisms for the observed responses by taking into account loss factors such as grazing and viral lysis. These aspects in combination with our focus on the smaller-sized phytoplankton contributed largely to a more detailed and inclusive understanding of ecological responses to changes in CO₂.

A shift towards the smallest phytoplankton as a result of OA will have direct consequences for the structure and functioning of the pelagic food web and thus for the biogeochemical cycles. Due to the very small cell size, one or two additional trophic levels of smaller grazers are evident, which will, as compared to the more traditional food chain (large phytoplankton, suspension-feeding zooplankton and fish), result in reduced transfer of matter and energy to higher predators and increased importance of the microbial food web. Furthermore, the dominant pico- and nanophytoplankton groups were found prone to viral lysis, thereby shunting the carbon that enters the biological pool via photosynthesis from carbon accumulation in living organisms into the dissolved pools of organic carbon (Suttle, 2007). Microbial communities incorporate these pools, thereby converting

much of it to CO₂ again by respiration and subsequently influencing the efficiency of the biological pump (Brussaard et al., 2008).

The here discussed ecological changes by OA do not stand alone as global climate change impacts the polar waters also through temperature rise, shift in wind, precipitation and circulation (Schofield et al., 2010). Phytoplankton growth-relevant factors such as light, *p*CO₂, temperature, nutrient availability and salinity are all under change due to global warming. The increment in surface water temperature will reduce the solubility of CO₂ in the Arctic seawater, and the mean cell size of the phytoplankton community (Daufresne et al., 2009). Moreover, increased surface water temperature and glacier and sea-ice melt will strengthen vertical stratification, which in the Canadian Arctic waters has been reported to stimulate picophytoplankton and reduce nanophytoplankton abundance (Li et al., 2009). Thus, in the global climate-driven changing Arctic Ocean, the smallest phytoplankton are expected to flourish as a general result of OA that is further reinforced in summer by increased temperature-imposed vertical stratification.

Acknowledgements. This work is a contribution to the “European Project on Ocean Acidification” (EPOCA), which received funding from the European Community’s Seventh Framework Programme (FP7/2007-2013) under grant agreement no. 211384. The research leading to these results has also received funding from the European Union Seventh Framework Program (FP7/2007-2-13) under grant agreement no. 228224, MESOAQUA. We gratefully acknowledge the logistical support of Greenpeace International for its assistance with the transport of the mesocosm facility from Kiel to Ny-Ålesund and back to Kiel. We also thank the captains and crews of *M/V ESPERANZA* of Greenpeace and *R/V Viking Explorer* of the University Centre in Svalbard (UNIS) for assistance during mesocosm transport and during deployment and recovery in Kongsfjorden. We thank the staff of the French–German Arctic Research Base at Ny-Ålesund (AWIPEV), in particular Marcus Schumacher, for on-site logistical support. We are indebted to Richard Bellerby for providing DIC data, Sebastian Krug for general support and Jan Czerny for his advice on the sampling of the mesocosms for phytoplankton losses. We finally thank Maarten van Loon for arranging accommodation at the Dutch Station.

Edited by: T. F. Thingstad

References

- Aberle, N., Schul, K. G., Stuhr, A., Ludwig, A., and Riebesell, U.: High tolerance of protozooplankton to ocean acidification in an Arctic coastal plankton community, *Biogeosciences*, accepted, 2013.
- Baudoux, A.-C. and Brussaard, C. P. D.: Influence of irradiance on viral-algal host interactions, *J. Phycol.*, 44, 902–908, 2008.
- Bellerby, R. G. J., Silyakova, A., Nondal, G., Slagstad, D., Czerny, J., De Lange, T., and Ludwig, A.: Marine carbonate system

- evolution during the EPOCA Arctic pelagic ecosystem experiment in the context of simulated future Arctic ocean acidification, *Biogeosciences*, in review, 2013.
- Boras, J. M., Montserrat Sala, M., Arrieta, J. M., Sa, E. L., Felipe, J., Agustí, S., Duarte, C. M., and Vaque, D.: Effect of ice melting on bacterial carbon fluxes channeled by viruses and protists in the Arctic Ocean, *Polar Biol.*, 1695–1707, 2010.
- Boyd, P. W. and Doney, S. C.: Modelling regional responses by marine pelagic ecosystems to global climate change, *Geophys. Res. Lett.*, 29, 1806, doi:10.1029/2001GL014130, 2002.
- Brussaard, C. P. D.: Optimization of procedures for counting viruses by flow cytometry, *Appl. Environ. Microbiol.*, 70, 1506–1513, 2004.
- Brussaard, C. P. D. and Martínez Martínez, J.: Algal bloom viruses, *Plant Viruses*, 2, 1–13, 2008.
- Brussaard, C. P. D., Gast, G. J., Van Duyl, F. C., and Riegman, R.: Impact of phytoplankton bloom magnitude on pelagic microbial food web, *Mar. Ecol. Prog. Ser.*, 144, 211–221, 1996.
- Brussaard, C. P. D., Mari, X., Van Bleijswijk, J. D. L., and Veldhuis, M. J. W.: A mesocosm study of *Phaeocystis globosa* population dynamics, II. Significance for the microbial community, *Harmful Algae*, 4, 875–893, 2005.
- Brussaard, C. P. D., Wilhelm, S. W., Thingstad, F., Weinbauer, M. G., Bratbak, G., Heldal, M., Kimmance, S. A., Middelboe, M., Nagasaki, K., Paul, J. H., Schroeder, D. C., Suttle, C. A., Vaqué, D., and Wommack, K. E.: Global-scale processes with a nanoscale drive: the role of marine viruses, *ISME J.*, 2, 575–578, 2008.
- Cuvelier, M. J., Allenc, A. E., Monier, A., McCrow, J. P., Messié, M., Tringe, S. G., Woyke, T., Welsh, R. M., Ishoey, T., Lee, J., Binder, B. J., DuPont, C. L., Latasa, M., Guigand, C., Buck, K. R., Hilton, J., Thiagarajan, M., Caler, E., Read, B., Lasken, R. S., Chavez, F. P., and Worden, A. Z.: Targeted metagenomics and ecology of globally important uncultured eukaryotic phytoplankton, *P. Natl. Acad. Sci.*, 107, 14679–14684, 2010.
- Daufresne, M., Lengfellner, K., and Sommer, U.: Global warming benefits the small in aquatic ecosystems, *P. Natl. Acad. Sci.*, 106, 12788–12793, 2009.
- De Kluijver, A., Soetaert, A., Czerny, J., Schulz, K. G., Boxhammer, T., Riebesell, U., and Middelburg, J.J.: A ^{13}C labelling study on carbon fluxes in Arctic plankton communities under elevated CO_2 levels, *Biogeosciences*, accepted, 2013.
- Engel, A., Schulz, K. G., Riebesell, U., Bellerby, R., Delille, B., and Schartau, M.: Effects of CO_2 on particle size distribution and phytoplankton abundance during a mesocosm bloom experiment (PeECE II), *Biogeosciences*, 5, 509–521, doi:10.5194/bg-5-509-2008, 2008.
- Falkowski, P. G., Barber, R. T., and Smetacek, V.: Biogeochemical Controls and Feedbacks on Ocean Primary Production, *Science*, 281, 200–206, 1998.
- Feng, Y., Hare, C. E., Leblanc, K., Rose, J. M., Zhang, Y., DiTullio, G. R., Lee, P. A., Wilhelm, S. W., Rowe, J. M., Sun, J., Nemcek, N., Gueguen, C., Passow, U., Benner, I., Brown, C., and Hutchins, D. A.: Effects of increased $p\text{CO}_2$ and temperature on the North Atlantic spring bloom. I. The phytoplankton community and biogeochemical response, *Mar. Ecol.-Prog. Ser.*, 388, 13–25, 2009.
- Fukuda, R., Ogawa, H., Nagata, T., and Koike, I.: Direct determination of carbon and nitrogen contents of natural bacterial assemblages in marine environments, *Appl. Environ. Microbiol.*, 64, 3352–3358, 1998.
- Gasol, J. M., Zweifel, U. L., Peters, F., Fuhrman, J. A., and Hagström, Å.: Significance of size and nucleic acid content heterogeneity as measured by flow cytometry in natural planktonic bacteria, *Appl. Environ. Microbiol.*, 65, 4475–4483, 1999.
- Giordano, M., Beardall, J., and Raven, J. A.: CO_2 concentrating mechanisms in algae: mechanisms, environmental modulation, and evolution, *Annu. Rev. Plant Biol.*, 56, 99–131, 2005.
- Hoegh-Guldberg, O. and Bruno, J. F.: The Impact of Climate Change on the World's Marine Ecosystems, *Science*, 328, 1523–1528, 2010.
- Hopkins, F. E., Turner, S. M., Nightingale, P. D., Steinke, M., Bakker, D., and Liss, P. S.: Ocean acidification and marine trace gas emissions, *Proc. Natl. Acad. Sci. USA*, 107, 760–765, 2010.
- Landry, M. R. and Hassett, R. P.: Estimating the grazing impact of marine micrzooplankton, *Mar. Biol.*, 67, 283–288, 1982.
- Lebaron, P., Servais, P., Agogué, H., Courties, C., and Joux, F.: Does the high nucleic acid content of individual bacterial cells allow us to discriminate between active cells and inactive cells in aquatic systems?, *Appl. Environ. Microbiol.*, 67, 1775–1782, 2001.
- Li, W. K. W., McLaughlin, F. A., Lovejoy, C., and Carmack, E. C.: Smallest algae thrive as the Arctic Ocean freshens, *Science*, 326, 5952, doi:10.1126/science.1179798, 2009.
- Marie, D., Brussaard, C. P. D., Partensky, F., and Vaulot, D.: Enumeration of phytoplankton, bacteria and viruses in marine samples, in: *Current protocols in cytometry*, edited by: Robinson, J. P., Darzynkiewicz, Z., Dean, P. N., Rabinovitch, P. S., Stewart, C. C., Tanke, H. J., and Wheelless, L. L., John Wiley and Sons, 11.11.11–11.11.15, 1999.
- Meakin, N. G. and Wyman, M.: Rapid shifts in picoeukaryote community structure in response to ocean acidification, *ISME J.*, 5, 1397–1405, 2011.
- Middelboe, M., Nielsen, T. G., and Bjørnsen, P. K.: Viral and bacterial production in the North Water: in situ measurements, batch-culture experiments and characterization and distribution of a virus-host system, *Deep-Sea Res. II*, 49, 5063–5079, 2002.
- Motegi, C., Tanaka, T., Piontek, J., Brussaard, C. P. D., Gattuso, J. P., and Weinbauer, M. G.: Effect of CO_2 enrichment on bacterial production and respiration and on bacterial carbon metabolism in Arctic waters, *Biogeosciences*, in review, 2013.
- Newbold, L. K., Oliver, A. E., Booth, T., Tiwari, B., DeSantis, T., Maguire, M., Andersen, G., Van der Gast, C. J., and Whiteley, A. S.: The response of marine picoplankton to ocean acidification, *Environ. Microbiol.*, 14, 2293–2307, doi:10.1111/j.1462-2920.2012.02762.x, 2012.
- Parada, V., Herndl, G. J., and Weinbauer, M. G.: Viral burst size of heterotrophic prokaryotes in aquatic systems, *J. Mar. Biol. Ass. UK*, 86, 613–621, 2006.
- Paulino, A. I., Egge, J. K., and Larsen, A.: Effects of increased atmospheric CO_2 on small and intermediate sized osmotrophs during a nutrient induced phytoplankton bloom, *Biogeosciences*, 5, 739–748, doi:10.5194/bg-5-739-2008, 2008.
- Piontek, J., Borchard, C., Sperling, M., Schulz, K.G., Riebesell, U., and Engel, A.: Response of bacterioplankton activity in an Arctic fjord system to elevated $p\text{CO}_2$: results from a mesocosm perturbation study, *Biogeosciences*, in press, 2013.
- Riebesell, U. and Tortell, P. D.: Effects of ocean acidification on pelagic organisms and ecosystems, in: *Ocean Acidification*,

- Oxford University Press, Oxford, UK, 99–121, 2011.
- Riebesell, U., Schulz, K. G., Bellerby, R. G. J., Botros, M., Fritsche, P., Meyerhofer, M., Neill, C., Nondal, G., Oschlies, A., Wohlers, J., and Zollner, E.: Enhanced biological carbon consumption in a high CO₂ ocean, *Nature*, 450, 545–549, 2007.
- Riebesell, U., Czerny, J., von Bröckel, K., Boxhammer, T., Büdenbender, J., Deckelnick, M., Fischer, M., Hoffmann, D., Krug, S.A., Lentz, U., Ludwig, A., Mucche, R., and Schulz, K. G.: Technical Note: A mobile sea-going mesocosm system: New opportunities for ocean change research, *Biogeosciences*, in review, 2013.
- Rose, J. M., Feng, Y., Gobler, C. J., Gutierrez, R., Hare, C. E., Leblanc, K., and Hutchins, D. A.: Effects of increased pCO₂ and temperature on the North Atlantic spring bloom, II. Microzooplankton abundance and grazing, *Mar. Ecol. Prog. Ser.*, 388, 27–40, 2009.
- Rost, B., Zondervan, I., and Wolf-Gladrow, D.: Sensitivity of phytoplankton to future changes in ocean carbonate chemistry: current knowledge, contradictions and research directions, *Mar. Ecol. Prog. Ser.*, 373, 227–237, 2008.
- Ruardij, P., Veldhuis, M. J. W., and Brussaard, C. P. D.: Modelling the development and termination of a *Phaeocystis* bloom, *Harmful Algae*, 4, 941–963, 2005.
- Schofield, O., Ducklow, H. W., Martinson, D. G., Meredith, M. P., Moline, M. A., and Fraser, W. R.: How Do Polar Marine Ecosystems Respond to Rapid Climate Change?, *Science*, 328, 1520–1523, 2010.
- Schulz, K. G., Bellerby, R. G. J., Brussaard, C. P. D., Büdenbender, J., Czerny, J., Engel, A., Fischer, M., Koch-Klavnsen, S., Krug, S. A., Lischka, S., Ludwig, A., Meyerhöfer, M., Nondal, G., Silyakova, A., Stuhr, A., and Riebesell, U.: Temporal biomass dynamics of an Arctic plankton bloom in response to increasing levels of atmospheric carbon dioxide, *Biogeosciences*, 10, 161–180, doi:10.5194/bg-10-161-2013, 2013.
- Suffrian, K., Simonelli, P., Nejstgaard, J. C., Putzeys, S., Carotenuto, Y., and Antia, A. N.: Microzooplankton grazing and phytoplankton growth in marine mesocosms with increased CO₂ levels, *Biogeosciences*, 5, 1145–1156, doi:10.5194/bg-5-1145-2008, 2008.
- Suttle, C. A.: Marine viruses – major players in the global ecosystem, *Nat. Rev. Microbiol.*, 5, 801–812, 2007.
- The Royal Society: Ocean acidification due to increasing atmospheric carbon dioxide, Policy Document 12/05, Roy. Soc. Rep. 12, Royal Society, London, 2005.
- Tortell, P. D., DiTullio, G. R., Sigman, D. M., and Morel, F. M. M.: CO₂ effects on taxonomic composition and nutrient utilization in an Equatorial Pacific phytoplankton assemblage, *Mar Ecol. Prog. Ser.*, 23, 37–43, 2002.
- Tremblay, G., Belzile, C., Gosselin, M., Poulin, M., Roy, S., and Tremblay, J.-E.: Late summer phytoplankton distribution along a 3500 km transect in Canadian Arctic waters: strong numerical dominance by picoeukaryotes, *Aquat. Micr. Ecol.*, 54, 55–70, 2009.
- Vaqué, D., Casamayor, E. O., and Gasol, J. M.: Dynamics of whole community bacterial production and grazing losses in seawater incubations as related to the changes in the proportions of bacteria with different DNA content, *Aquat. Microb. Ecol.*, 25, 163–177, 2001.
- Veldhuis, M. J. W. and Kraay, G. W.: Phytoplankton in the subtropical Atlantic Ocean: Towards a better assessment of biomass and composition, *Deep-Sea Res.*, 51, 507–530, 2004.
- Wang, Y., Hammes, F., Boon, N., Chami, M., and Egli, T.: Isolation and characterization of low nucleic acid (LNA)-content bacteria, *ISME J.*, 3, 889–902, 2009.
- Waters, R. E. and Chan, A. T.: *Micromonas pusilla* virus: the virus growth cycle and associated physiological events within the host cells; host range mutation, *J. Gen. Virol.*, 63, 199–206, 1982.
- Weinbauer, M. G.: Ecology of prokaryotic viruses, *FEMS Microbiol. Rev.*, 28, 127–181, 2004.
- Worden, A. Z., Lee, J.-H., Mock, T., Rouzé, P., Simmons, M. P., Aerts, A. L., Allen, A. E., Cuvelier, M. L., Derelle, E., Everett, M. V., Foulon, E., Grimwood, J., Gundlach, H., Henrisat, B., Napoli, C., McDonald, S. M., Parker, M. S., Rombauts, S., Salamov, A., Von Dassow, P., Badger, J. H., Coutinho, P. M., Demir, E., Dubchak, I., Gentemann, C., Eikrem, W., Gready, J. E., John, U., Lanier, W., Lindquist, E. A., Lucas, S., Mayer, K. F. X., Moreau, H., Not, F., Otilar, R., Panaud, O., Pangilinan, J., Paulsen, I., Piegu, B., Poliakov, A., Robbens, S., Schmutz, J., Toulza, E., Wyss, T., Zelensky, A., Zhou, K., Armbrust, E. V., Bhattacharya, D., Goodenough, U. W., Van de Peer, Y., and Grigoriev, I. V.: Green Evolution and Dynamic Adaptations Revealed by Genomes of the Marine Picoeukaryotes *Micromonas*, *Science*, 324, 268–272, 2009.
- Zhu, F., Massana, R., Not, F., Marie, D., and Vault, D.: Mapping of picoeukaryotes in marine ecosystems with quantitative PCR of the 18S rRNA gene, *FEMS Microb. Ecol.*, 52, 79–92, 2005.
- Zubkov, M. V., Fuchs, B. M., Burkhill, P. H., and Amann, R.: Comparison of Cellular and Biomass Specific Activities of Dominant Bacterioplankton Groups in Stratified Waters of the Celtic Sea, *Appl. Environ. Microbiol.*, 67, 5210–5218, 2001.